JGR Space Physics

RESEARCH ARTICLE
10.1029/2019JA027054

Oxygen Ion Flow Reversals in Earth's Magnetotail: A Cluster Statistical Study

A. De Spiegeleer[1], M. Hamrin[1], M. Volwerk[2], T. Karlsson[3], H. Gunell[1,4], G. S. Chong[1], T. Pitkänen[1,5], and H. Nilsson[6]

[1]Department of Physics, Umeå University, Umeå, Sweden, [2]Space Research Institute, Austrian Academy of Sciences, Graz, Austria, [3]Space and Plasma Physics, School of Electrical Engineering and Computer Science, KTH Royal Institute of Technology, Stockholm, Sweden, [4]Belgian Institute for Space Aeronomy, Brussels, Belgium, [5]Shandong Provincial Key Laboratory of Optical Astronomy and Solar-Terrestrial Environment, Institute of Space Sciences, Shandong University, Weihai, China, [6]Swedish Institute of Space Physics, Kiruna, Sweden

Key Points:
- Flow reversals from earthward to tailward can be due to an enhanced flux of earthward moving particles which move tailward after mirroring
- Flow reversals can be flux enhancements for which the pitch angle changes from 0° (180°) to 180° (0°) in the Northern (Southern) Hemisphere
- The particles forming the flow reversals have typically traveled $<25R_E$ from the apparent source to the spacecraft

Supporting Information:
- Supporting Information S1

Correspondence to:
A. De Spiegeleer,
alexandre.de.spiegeleer@umu.se

Citation:
De Spiegeleer, A., Hamrin, M., Volwerk, M., Karlsson, T., Gunell, H., Chong, G. S., et al. (2019). Oxygen ion flow reversals in Earth's magnetotail: A Cluster statistical study. *Journal of Geophysical Research: Space Physics*, *124*, 8928–8942. https://doi.org/10.1029/2019JA027054

Received 20 JUN 2019
Accepted 22 OCT 2019
Accepted article online 13 NOV 2019
Published online 21 NOV 2019

Abstract We present a statistical study of magnetotail flows that change direction from earthward to tailward using Cluster spacecraft. More precisely, we study 318 events of particle flux enhancements in the O^+ data for which the pitch angle continuously changes with time, either from 0° to 180° or from 180° to 0°. These structures are called "Pitch Angle Slope Structures" (PASSes). PASSes for which the pitch angle changes from 0° to 180° are observed in the Northern Hemisphere while those for which the pitch angle changes from 180° to 0° are observed in the Southern Hemisphere. These flux enhancements result in a reversal of the flow direction from earthward to tailward regardless of the hemisphere where they are observed. Sometimes, several PASSes can be observed consecutively which can therefore result in oscillatory velocity signatures in the earth-tail direction. The PASS occurrence rate increases from 1.8% to 3.7% as the AE index increases from ~0 to ~600 nT. Also, simultaneously to PASSes, there is typically a decrease in the magnetic field magnitude due to a decrease (increase) of the sunward component of the magnetic field in the Northern (Southern) Hemisphere. Finally, based on the 115 (out of 318) PASSes that show energy-dispersed structures, the distance to the source from the spacecraft is estimated to be typically $<25R_E$ along the magnetic field line. This study is important as it sheds light on one of the causes of tailward velocities in Earth's magnetotail.

1. Introduction

The description of the dynamics of the Earth's magnetosphere as described by the Dungey cycle (Dungey, 1961) is oversimplifying in many ways. For example, the textbook Dungey cycle suggests that, earthward of nightside magnetic reconnection, only earthward flows are expected to exist. However, there have been numerous reports of tailward flows in the region of closed field lines in the near Earth's magnetotail. Such tailward flows disagree with the conventional convection pattern depicted by the Dungey cycle, and the origin of these flows must be explained.

The tailward flows on closed field lines in the magnetotail have usually been studied by using the plasma velocity perpendicular to the magnetic field or by using the total velocity vector (e.g. Birn et al., 2011; Juusola et al., 2011; Panov et al., 2010; Pitkänen et al., 2011). And these studies have used either proton (H^+) data or have not distinguished between the different ion species. On the other hand, tailward flows can sometimes be observed along the magnetic field not only in H^+ data but also in oxygen ion (O^+) data such as for beams in the plasma sheet boundary layer (Eastman et al., 1984). In addition, tailward flows are sometimes closely related to earthward flows. This may be the case for some velocity oscillations observed by spacecraft in the Earth's magnetotail plasma sheet. These velocity oscillations may have various causes.

Among the common causes for velocity oscillations are magnetohydrodynamic waves for which the velocity oscillates with the fields, for example, the Alfvén waves, the magnetosonic waves, the flapping waves, and the kink waves (e.g., Alfvén, 1943; Roberts, 1981; Sergeev et al., 2004; Turkakin et al., 2014). In addition, velocity oscillations can also be observed when earthward propagating high-speed flows reach the region dominated by Earth's magnetic dipole (e.g., Panov et al., 2010, 2014). For instance, the high-speed flows may overshoot the equilibrium position between the dipolar region and the magnetotail. This would result

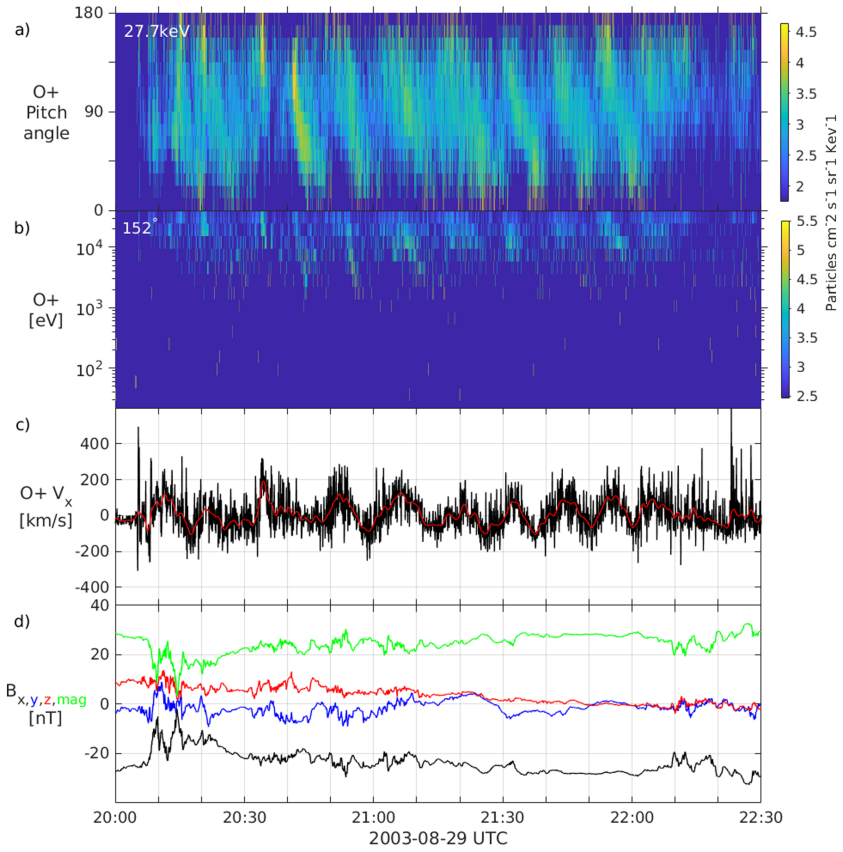

Figure 1. Cluster 4 data on 29 August 2003. (a) O^+ pitch angle-time spectrogram at 27.7 keV. (b) O^+ energy-time spectrogram at 152° pitch angle. (c) O^+ velocity moment in V_X and (d) magnetic field data (Geocentric Solar Ecliptic coordinate system). The particle data are from the CIS-CODIF instrument and the magnetic field data from the FluxGate Magnetometer instrument.

in a heavily damped oscillation of the high-speed flow in the earth-tail direction. Another possibility to observe consecutive earthward-tailward flows is the repeated crossings of an X-line (e.g., Eastwood et al., 2010). When the spacecraft is earthward (tailward) of the X-line, earthward (tailward) flows are observed. Therefore, if an X-line and the spacecraft move relative to each other in the earth-tail direction, velocity oscillations will be observed in the same direction.

Recently, two oscillatory flows that change direction from earthward to tailward (De Spiegeleer et al., 2019) observed in the O^+ velocity moment have been reported to be due to repeated particle flux enhancements along the magnetic field. Enhancements similar to those of the O^+ could sometimes be discerned in the H^+ data but they were not as clear and the focus was therefore upon the O^+ data. We show the most important characteristics of such phenomenon in Figure 1, and we will present them in greater detail in section 2.2. The pitch angle of the enhancements had the characteristic of continuously and repeatedly changing from approximately 0° to 180° in the Northern Hemisphere and from 180° to 0° in the Southern Hemisphere (Figure 1a). Because the observations were from the magnetotail around midnight where the direction of the magnetic field is mainly in the X direction, the oscillations along the magnetic field corresponded mostly to earthward-tailward flows (Figure 1c).

A single, continuous change in pitch angle is explained as follows (see De Spiegeleer et al., 2019, for more details). A source located tailward of the spacecraft energizes a distribution of particles. The particles move along the field lines with a field-aligned speed that depends on the particles' energy and pitch angle. The particles are then reflected at their mirror point and start moving tailward. A spacecraft situated on the particles' trajectory and measuring the particles with a particular energy would observe earthward moving particles with pitch angle becoming more perpendicular as time increases. This is because the more perpendicular particles have lower field-aligned speed. Then, the spacecraft starts measuring the particles after they have

mirrored, that is, the tailward moving particles. Such signatures were observed in the pitch angle-time spectrogram and were referred to as "Pitch Angle Slope Structure" (PASS). Each of these PASSes corresponded to the reversal of the flow that changes from earthward to tailward. Repeated PASSes therefore resulted in oscillatory flows in the earth-tail direction.

In this article, our focus is on O^+ PASSes because, as mentioned in De Spiegeleer et al. (2019), they appear to be clearer than H^+ PASSes. O^+ PASSes are statistically investigated to reveal their typical properties. For instance, we aim to answer the following questions. Are PASSes really due to particles moving over the spacecraft, or could the spacecraft be moving over a spatial structure? How often are PASSes observed? Where and under which conditions are they more favorably observed? Additional O^+ populations than the O^+ PASS population may be present. Therefore, we also investigate whether or not the PASS population is dominant enough to result in a reversal of the bulk velocity along the magnetic field. Can H^+ PASSes be observed together with O^+ PASSes? Where do the particles forming PASSes come from?

2. Data and Event Selection

2.1. Data

We use particle data from the Cluster Ion Spectrometry-COmposition DIstribution Function (CIS-CODIF) instrument (Rème et al., 2001) aboard Cluster 4 (C4) (Escoubet et al., 2001) during the tail seasons (1 June till 1 December) of the years 2001–2003. The CIS-CODIF instrument distinguishes between ion species, and we use the oxygen (O^+) and proton (H^+) data. The pitch angle distribution (PAD) (i.e., the particle flux as a function of the pitch angle and the energy) of O^+ is used. PAD data presented as spectrogram will either be referred to as "energy-time spectrogram" or "pitch angle-time spectrogram" when presented at constant pitch angle or energy, respectively. We also use the magnetic field data from the FluxGate Magnetometer instrument (Balogh et al., 2001). Finally, we use the AE index (Davis & Sugiura, 1966) data. Unless otherwise stated, all vectorial quantities are in the Geocentric Solar Ecliptic coordinate system.

2.2. Sample Event

In this section, we aim to give the reader a better feeling for the PASSes that are described in the introduction as they are the core of this statistical study. In Figure 1, we show the most important properties of the PASSes observed in the Southern Hemisphere as presented in De Spiegeleer et al. (2019). The main differences between the Northern and Southern Hemisphere events are mentioned at the end of the section.

At least seven clear PASSes can be seen in the pitch angle-time spectrogram of O^+ observed by Cluster 4 shown in Figure 1a. The first one starts at about 20:40 UTC on 29 August 2003 and has a duration of less than 10 min. The last PASS starts at 21:52 UTC and finishes at 22:00 UTC. For each of the seven PASSes observed between 20:40 UTC and 22:00 UTC, the particle flux enhancement is first seen at a pitch angle relatively close to 180°. The enhancement then gradually shifts to lower pitch angles until it reaches ∼0°. Note that each PASS has this same characteristic, and no enhancements of the particle flux is seen to smoothly change pitch angle back from 0° to 180° between each PASSes.

During the whole duration of the PASSes, the magnetic field data ($B_X < 0$ in Figure 1d) indicate that Cluster 4 was continually below the neutral sheet. The magnetic field also shows that the magnetotail was relatively stretched. Therefore, a particle with 180° pitch angle moves toward Earth while a particle with 0° pitch angle moves away from Earth. Hence, the enhancements seen in the pitch angle-time spectrogram can be interpreted as particles first moving toward Earth over the spacecraft and smoothly changing into particles moving away from it. These signatures in the distribution function naturally affect the velocity moment, and the effect can clearly be seen in the Earth-Sun direction as shown in Figure 1c.

In addition, energy-dispersed signatures in the energy-time spectrogram were observed together with PASSes. These are shown in Figure 1b. The particle flux enhancements decreased in energy with time. From these observations, it was deduced that the location of the source was between ∼5 and ∼25 R_E away from the satellite. The estimated distance varied significantly between the different PASSes.

De Spiegeleer et al. (2019) also presented a similar event but it was observed in the Northern Hemisphere. A few differences between the Northern and Southern Hemisphere events are summarized below as they highlight the need for this statistical study.

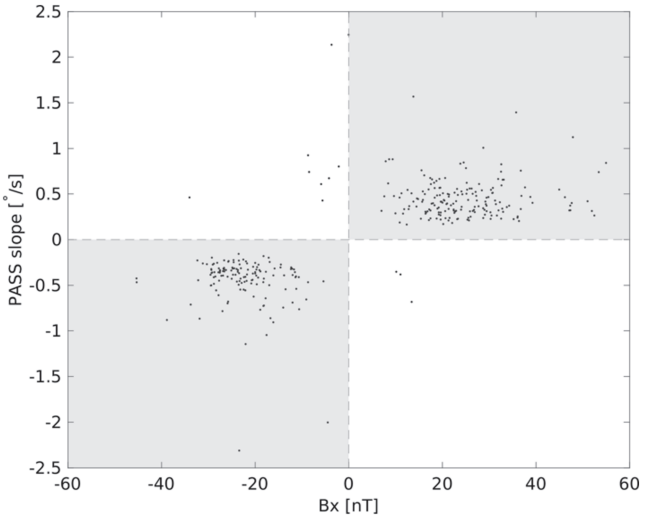

Figure 2. Scatter plot of the slope of each PASS in the pitch angle-time spectrogram against B_X. $B_X > 0$ is used as a proxy to identify the Northern Hemisphere while $B_X < 0$, the Southern Hemisphere.

1. The PASSes observed in the Northern Hemisphere show a change in pitch angle from 0° to 180° while those in the Southern Hemisphere show a change in pitch angle from 180° to 0°.
2. Only three PASSes were observed in the Northern Hemisphere event, and the times between each of them do not seem constant as is the case for the Southern Hemisphere event.
3. For the Northern Hemisphere event, the estimated distance to the source from the spacecraft varied between ~40 and ~100R_E while the distance to the source for the Southern Hemisphere event ranged between 5 and 25 R_E.
4. All seven PASSes observed in the Southern Hemisphere show energy-dispersed structure while only two of the three PASSes in the Northern Hemisphere show energy-dispersed structure.

2.3. Event Selection

This statistical study is based upon the selection of O^+ particle flux enhancements in the pitch angle-time spectrogram in the highest energy channel of CIS-CODIF (35.2 keV energy channel corresponding to the energy range between 30.2 and 38.5 keV). An enhancement must show a clear increase or decrease in the pitch angle as a function of time. Because the selection is done manually, we provide the exhaustive list of events in the supporting information Table S1. The following criteria are used to select the events.

1. We plot by 6 hr time interval the O^+ pitch angle-time spectrogram for the five highest energy channels (energy range: 11.5–38.5 keV) as well as the spacecraft position.
2. We only take into account the tail region: $X < -10R_E$ and $|Y| < 10R_E$.
3. We look for particle flux enhancements for which the pitch angle changes either from ~0° to 180° or from ~180° to 0° with time, that is, observations similar to figures 3d and 6c in De Spiegeleer et al. (2019).
4. The event is selected if the particle flux before and after the potential event is relatively steady.
5. Consecutive enhancements are allowed, and each individual enhancement is selected separately.
6. We select the beginning and ending of the enhancements in the pitch angle-time spectrogram.

A total of 330 events (PASSes) are selected based upon these criteria. We intend to investigate events similar to those presented by De Spiegeleer et al. (2019). Therefore, we want to make sure that some basic properties of our selected events are similar to those presented in De Spiegeleer et al. (2019). It was suggested that the slope of a PASS in the pitch angle-time spectrogram depends on the hemisphere where they are observed. The slope is shown against the X component of the magnetic field, B_X, at the beginning of each PASS in Figure 2. The Northern (Southern) Hemisphere has $B_X > 0$ ($B_X < 0$), and the slope is calculated from a linear fit of the selected initial and final points in the pitch angle-time spectrogram.

We observe that a majority of the selected PASSes have structures similar to the two events presented by De Spiegeleer et al. (2019). Those with positive slopes are mostly observed in the Northern Hemisphere ($B_X > 0$) while those with negative slopes are observed in the Southern Hemisphere ($B_X < 0$). Therefore, for consistency purposes, we refine the amount of PASSes to those satisfying the dependence of the pitch angle slope on the hemisphere; 318 PASSes remain. The exhaustive list of the selected events can be found in Table S1. From the hemispheric dependence of the PASSes' slopes, De Spiegeleer et al. (2019) suggested that PASSes are temporal variations resulting from the arrival of newly emitted particles from a source tailward of the spacecraft. Similarly, we assume that PASSes are due to temporal variations, but we also discuss the possibility that PASSes result from spatial structures in section 4.1.

3. Observations

A number of PASS properties will hereafter be investigated. First, we investigate general properties of PASSes such as their time duration and their repeatedness as well as the locations where they are observed. Second, we look at the correlation between the PASSes and the state of the magnetosphere by using AE index. We observe that the occurrence rate of PASSes increase with the AE index up till AE ~600 nT. Third, we use

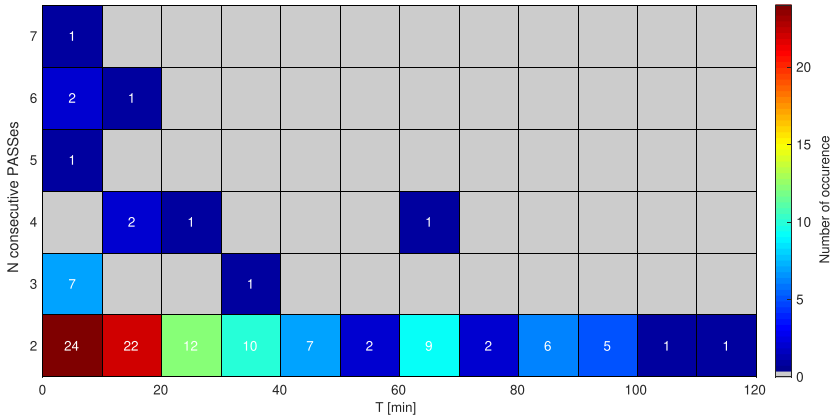

Figure 3. Number of occurrence of consecutive PASSes separated by T min. Consecutive PASSes range from two PASSes to seven PASSes.

the superposed epoch analysis method to verify that, as in De Spiegeleer et al. (2019), the enhancements of the particle flux result in the reversal of the velocity moment along the magnetic field. Hence, the repeated PASSes may appear as oscillations in the velocity moments. Fourth, we show that the magnetic field magnitude, B, as well as B_X have characteristic variations during the events. Fifth, we evaluate the distance along the field line between the spacecraft and where the particles are energized by using the energy-time spectrograms. We use the events which have energy-dispersed structure to evaluate the distance traveled by the particles along the magnetic field since they were accelerated. That distance is estimated to be typically less than 25 R_E.

3.1. Time Duration, Repeatedness, and Location

The duration of the selected events is typically between 4.0 and 6.4 min (25th and 75th percentiles) and have a median duration of 5.1 min. Note that these values are mostly indicative of the selection method rather than indicative of the actual particles dynamics. Indeed, very large or very small slopes in the pitch angle-time spectrogram might not have been identified and selected.

Both of the time periods presented by De Spiegeleer et al. (2019) contain several consecutive PASSes. Is this a common feature? We investigate how common it is to observe consecutive PASSes by showing, in Figure 3, the number of N-consecutive PASSes within T min from each other. For example, if we require a maximum time difference between the end of a PASS and the start of the next PASS to be 10 min, we find 24 occurrences of two consecutive PASSes, seven occurrences of three consecutive PASSes, one occurrence of five consecutive PASSes, two occurrences of six consecutive PASSes, and one occcurrence of seven consecutive PASSes. PASSes are exclusively counted, that is, PASSes counted in one set of consecutive PASSes cannot be part of another set of consecutive PASSes.

Out of the 318 PASSes, 202 are within a maximum of 40 min of another PASS. Hence PASSes are typically not observed as a single isolated structure but with at least one other PASS in its close surrounding. What occurs the most is the observation of two consecutive PASSes that are separated by 40 min or less. Such observations of two consecutive PASSes separated by less than 40 min add up to a total of 136 PASSes. We note also that more than two PASSes in a row can be observed and they are typically separated by less than 10 min. No more than seven consecutive PASSes are found. The number of observed consecutive PASSes decreases as the time between the PASSes increases.

PASSes that are observed soon after each other are expected to be related to each other. The study of consecutive PASSes may shed light on some properties of the source(s) of PASS particles. So the follow up question is: Are the consecutive PASSes due to temporal or spatial characteristics of the source? We shortly discuss the possibilities in section 4.1.

Then, we investigate where in the magnetotail, the PASSes are observed. This is done by binning the occurrence rate of PASSes in space (XY, YZ, and XZ planes; Figure S2) and for various plasma proton β values (Figure 4). For each bin, we compute the occurrence rate of PASSes (Figure 4a) by taking the ratio between

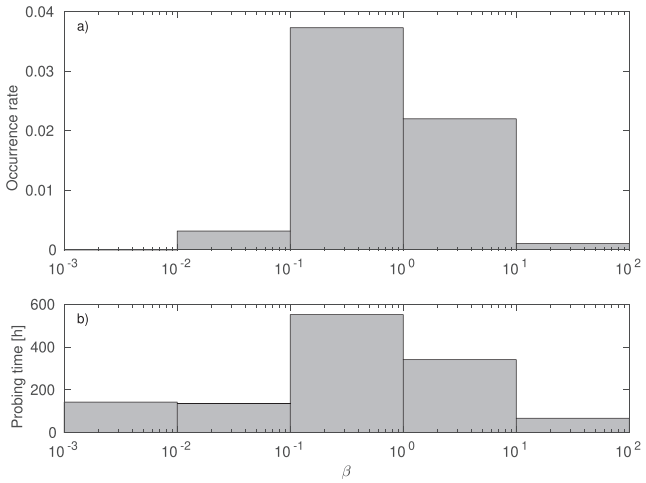

Figure 4. (a) Occurrence rate of PASSes as a function of proton β. (b) The normalization time, that is, the probing time, only includes time when the O^+ number density is > 0.005 cm^{-3}.

the time C4 observed PASSes by the total time during which C4 was in the bin. Because O^+ is not always present, we only consider the time when O^+ number density is above 0.005 cm^{-3} as normalizing time (Figure 4b). From the occurrence rate of PASSes in the *XY*, *XZ*, and *YZ* planes (Figure S2a–S2c), there is no preferred region where PASSes are more frequently observed. The results show that PASSes are mostly observed in the region where $0.1 \leq \beta < 10$ with an occurrence rate of 0.02–0.03. The closer C4 is to the neutral sheet, the larger β is. This means that PASSes can be observed on closed field lines in most of the plasma sheet but not much in the very center of the plasma sheet where the plasma $\beta > 10$ nor in the lobe region (Baumjohann et al., 1989).

3.2. Magnetospheric Conditions

The presence and effect of a number of plasma phenomena in the magnetotail can be observed in ground measurements. Therefore, we investigate the occurrence rate of PASSes as a function of the AE index (Figure 5a). Here, the occurrence rate is defined as the ratio between the time C4 observes PASSes for a defined AE interval and the total C4 probing time for the same AE interval. Again, because the presence of O^+ in the magnetosphere depends on the state of the magnetosphere, we must take into account only the time when O^+ is present and therefore require that O^+ number density >0.005 cm^{-3} for the normalizing time. The normalizing time is shown in Figure 5b.

The occurrence rate gradually increases from about 1.8% to 3.7% when AE increases from the [0, 100] nT range to [500, 600] nT. This shows that PASSes are observed more frequently when stronger perturbations of the horizontal ionospheric current are observed. Then, for larger values of AE, the occurrence rate drops to about 2% but remains stable up till 1,200 nT even though the probing time decreases significantly. It is unclear why this drop occurs, but we note that the probing decreases quickly indicating larger error on the occurrence rate estimates.

3.3. Velocity Moments

The events selected in this study (PASSes) are selected because of their characteristic signatures observable in the PAD data. If the particle flux of a PASS is large enough compared to the background O^+ populations, the effect of PASS particles should be reflected in the velocity moments in the form of a reversal of the velocity along the magnetic field.

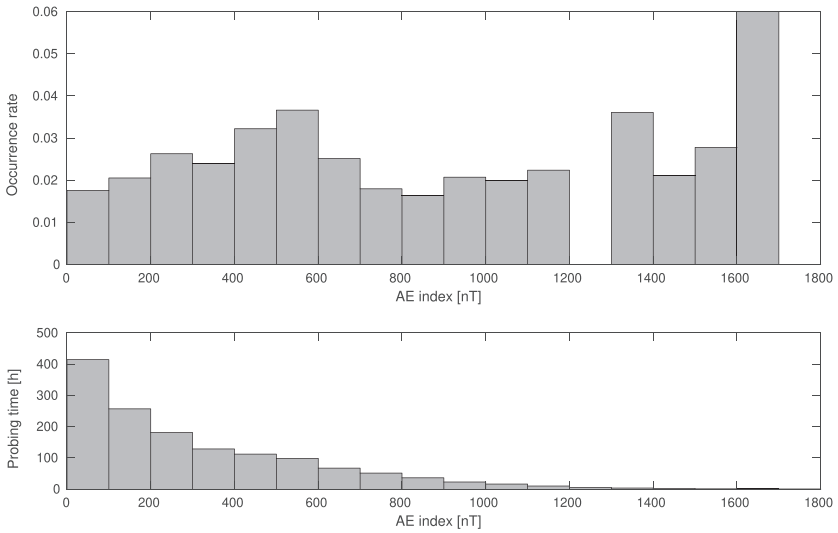

Figure 5. (a) PASS occurrence rate as a function of the AE index. (b) C4 probing time is used as the normalization time as a function of AE. It only includes time periods when O^+ number density is >0.005 cm^{-3}.

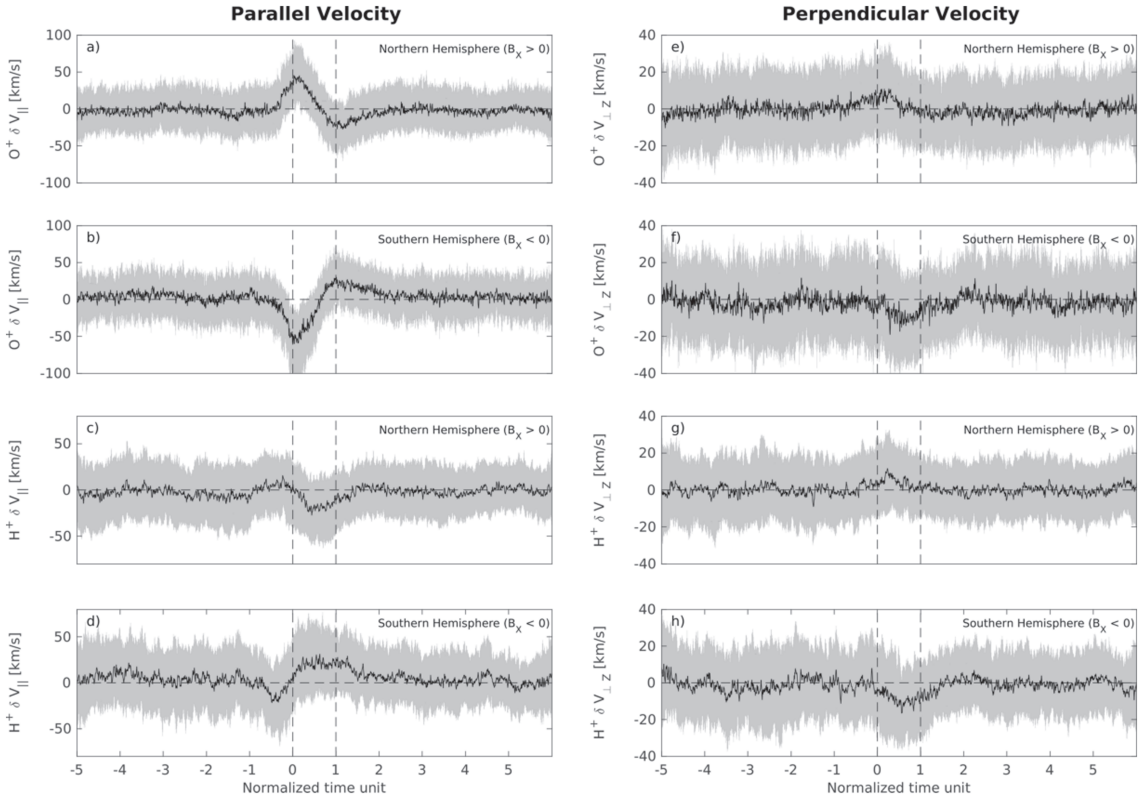

Figure 6. Superposed epoch analysis of the deviation of O^+ (a, b) and H^+ (c, d) parallel velocity from the background. The PASSes are between normalized time unit 0 and 1. Panels a and c show the Northern Hemisphere data while panels b and d show the Southern Hemisphere data.

This can be investigated using the superposed epoch analysis method. The idea behind it is to overlap the data (e.g., velocity and magnetic field data) associated with each PASS on top of each other and show the 25th, 50th (the median), and 75th percentiles at each time stamp to highlight the typical behavior of the superposed quantity. The range from the 25th and 75th percentiles are gray areas, and the median is a black line in the superposed epoch analysis plots (e.g., Figure 6). However, because the events have different time duration, the data must first be normalized in time so that each PASS has the same duration of 1 normalized time unit. The PASSes start at $t = 0$ and end at $t = 1$. We show five normalized time units before and after the event. Also, before calculating the 25th, 50th, and 75th percentiles, we remove the background trend of the data that is to be superposed. This is done by performing a second-order fit of the data from which we have removed the time interval of the PASS.

The superposed epoch analysis of the deviation of the parallel component of the O^+ velocity from the background ($O^+\delta V_{\parallel}$) in both Northern and Southern Hemispheres are shown in Figures 6a and 6b, respectively. Results show that the velocity signatures of PASSes in the Northern Hemisphere and Southern Hemisphere are opposite to each other. This is due to the opposite magnetic field configuration in the hemispheres.

In the Northern Hemisphere (Figure 6a), we see that $O^+\delta V_{\parallel}$ is positive at the beginning and negative at the end of PASS. The opposite is observed in the Southern Hemisphere (Figure 6b). These signatures correspond to a reversal of the flow direction in the parallel velocity from earthward to tailward, regardless of the hemisphere. In both hemispheres, the peak in earthward speed is slightly smaller than 50 km/s while the peak in the tailward speed is about 25 km/s. The lower tailward speed may be due to the diffusion of the particles in space as they travel back to the spacecraft location after their reflection at their mirror points. The particles, now moving tailward, have had more time to spread in space which may result in the spacecraft measuring a lower particle flux, therefore contributing less to the velocity moments.

Weaker but similar signatures are also observed in the H^+ parallel velocity (Figures 6c and 6d), suggesting that O^+ PASS is often accompanied by H^+ PASS (De Spiegeleer et al., 2019). The reversal signatures in the H^+ data are observed before those in O^+ data. This is fully expected considering that PASSes are due to the

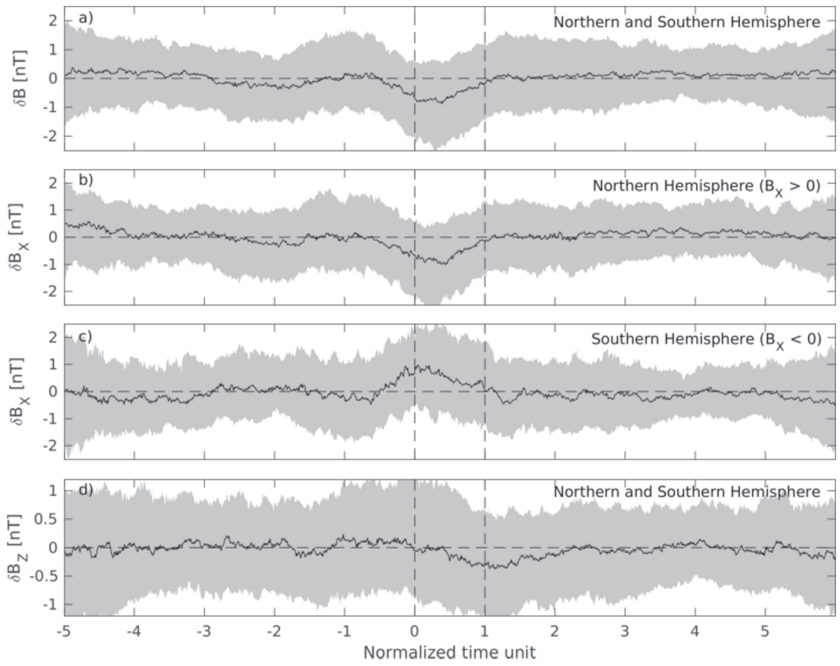

Figure 7. Superposed epoch analysis of the deviation of (a) B, (b) B_X in the Northern Hemisphere, (c) B_X in the Southern Hemisphere, and (d) B_Z from the background. PASSes are observed between normalized time unit 0 and 1.

time-of-flight effect and that H^+ particles are faster than O^+ particles. Also, the H^+ signatures are weaker than those of O^+ because the event selection is done based on O^+ PASSes and not H^+ PASSes. Hence, the start and the end of each reversal of H^+ $V_{\parallel}$ are not simultaneous, therefore resulting in weaker signatures shown in Figures 6c and 6d.

In addition to the reversal of the flow direction from earthward to tailward, variations are also present in the perpendicular velocity in the Z direction ($\delta V_{\perp Z}$). We show the result of the superposed epoch analysis of $\delta V_{\perp Z}$ for O^+ in Figures 6e and 6f and for H^+ in Figures 6g and 6h in the Northern and Southern Hemispheres. Regardless of the hemisphere, the observations for O^+ and H^+ are similar. In the Northern Hemisphere (Figures 6e and 6g), there is a peak in $\delta V_{\perp Z}$ around normalized time unit 0 which recovers to the typical value by normalized time unit 1. Oppositely in the Southern Hemisphere (Figures 6f and 6h), a decrease in $\delta V_{\perp Z}$ peaking around normalized time unit 0.5 is observed. These characteristic signatures will be discussed together with the magnetic field signatures (section 3.4) in section 4.3.

3.4. Magnetic Field

Figure 7 shows the superposed epoch analysis of the deviation from the background value of the magnitude of the magnetic field, B, B_X, as well as B_Z. The X component is separated between the Northern and Southern Hemispheres because the signatures are opposite. No consistent pattern can be identified in B_Y; hence, it is not shown.

As observed in Figure 7a, B decreases compared to its background value by about 0.9 nT near the beginning of PASS. Then, it recovers to the background value by the end of PASS. This change in magnitude is due to a change in B_X as can be seen in Figures 7b and 7c. In the Northern Hemisphere, B_X decreases first by about 1 nT and recovers to the background value by the end of PASS. The opposite is observed in the Southern Hemisphere. Finally, there may be a small decrease of about 0.4 nT in B_Z (Figure 7d, note the difference in the y axis) with a minimum at the end of the event. Note that these signatures observed in the magnetic field are weak, but they are seen not only in the median value but also in the 25th and 75th percentiles which may suggest that the signature is significant. Even though the trends are weak, they indicate that PASSes are related to the variations in the magnetic field. We interpret the magnetic field signatures in section 4.3.

3.5. Distance to the Source

Our interpretation that a PASS results from a temporal structure (section 4.1) implies that, due to the time-of-flight effect, there is a time delay between the observations of the particles depending on their

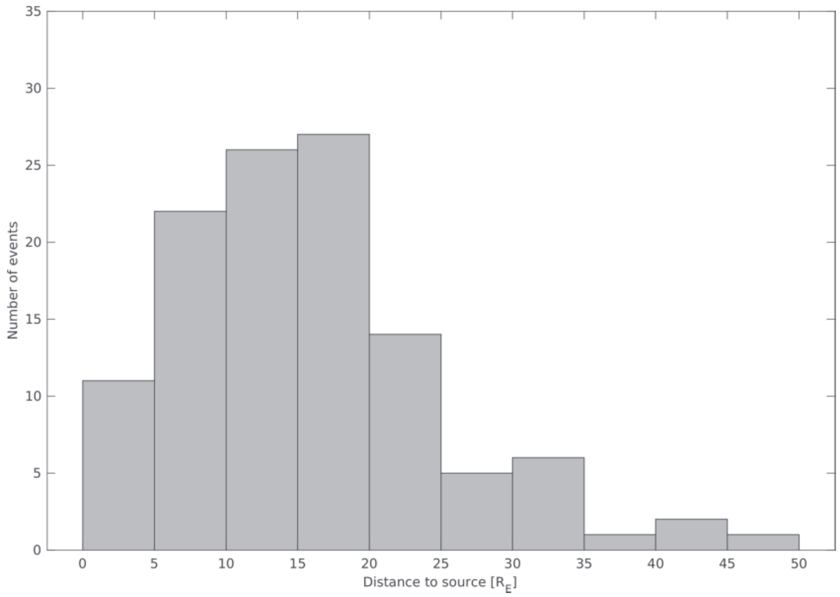

Figure 8. Histogram of the estimated distance to the source from the spacecraft position along the magnetic field line using the energy-dispersed signatures associated with PASSes in the energy-time spectrograms.

energy and pitch angle. The larger the field-aligned velocity, the faster the particle reaches the spacecraft. The time delay between the arrival of the particles with the same pitch angle but different energies result in energy-dispersed structure (particles with lower energies are observed later) in the energy-time spectrogram.

These dispersive signatures can be used to evaluate where the particles were energized (see, e.g., De Spiegeleer et al., 2019; Sauvaud & Kovrazhkin, 2004). Therefore, we visually inspect which PASSes have an energy-dispersed structure in the energy-time spectrogram and evaluate the distance to the source for each of them. The distance to the source is estimated using the most field-aligned particles (as they are less affected by, e.g., the field line convection, De Spiegeleer et al., 2019) for which the energy-dispersed structure is observed. This is done by linearly fitting the dispersion in the $1/V_{\parallel}$-time spectrogram. Because the particles move along the magnetic field lines and because we fit the dispersion in the $1/V_{\parallel}$-time spectrogram, our estimated distance to the source is the distance along the magnetic field line. It is important to note the assumptions made when evaluating the distance to the source using the time-of-flight effect. We assume that the magnetic field is constant along the particle trajectory and that the particles are not affected by any external forces between the source and the observation point.

Of the 318 PASSes, 115 show energy-dispersed structures. The rest of the events do not show clear dispersive signatures. One possible reason may be that there is a background population which makes it difficult to identify the dispersive signatures when plotting the PAD data as energy-time spectrograms. The results of the fitting of the energy-dispersed structures are shown in Figure 8. The results show that, for a majority of the events (100 out of 115), the particles have to travel $25R_E$ or less to produce the observed energy-dispersed structure, but in some cases (15 events), longer distances are necessary.

4. Summary and Discussion

In this study, we selected a total of 318 events showing particle flux enhancements of O^+ at 35.2 keV for which the pitch angle changes from 0° to 180° or from 180° to 0°. Such a signature is referred to as "Pitch Angle Slope Structure" (PASS). The main observations are summarized as follow.

1. PASSes are separated into two categories (gray quadrants of Figure 2). In the Northern Hemisphere, the pitch angle changes from ~ 0° to ~180°, and it changes from ~180° to ~0° in the Southern Hemisphere.
2. PASSes are observed on closed field lines ($0.1 \leq \beta < 10$, Figure 4).
3. PASSes result in the reversal of O^+ parallel velocity (Figure 6). The O^+ first travel earthward and then tailward. This feature is also observed in the H^+ velocity parallel to the magnetic field, suggesting that the mechanism that accelerates O^+ also accelerates H^+.

4. Consecutive PASSes are sometimes observed (Figure 3). When the PASSes are observed consecutively, oscillatory flows are observed (De Spiegeleer et al., 2019).
5. PASSes seem to be increasingly observed when the magnetosphere is more active as suggested by the PASSes occurrence rate as a function of AE index (Figure 5).
6. A depression in the magnetic field magnitude is typically observed simultaneously to the observations of PASSes. The depression is dominantly due to a decrease (increase) of B_X in the Northern (Southern) Hemispheres (Figure 7).
7. The source of the particles forming the PASSes is typically closer than 25 R_E away from the spacecraft along the field line (Figure 8).

The distance along the magnetic field between the spacecraft and the source was estimated using the energy-dispersed signatures. These estimations rely on the presumption that a PASS is due to the arrival of particles at the spacecraft position, that is, due to temporal variations (see section 4.1). The estimated distance varies between a few R_E up to about 50 R_E. It is not straightforward to identify where the source exactly is as it depends on the magnetic configuration of the magnetosphere. These distances may correspond to the distant tail in the case of a stretched magnetotail or to the ionospheric footpoint in the hemisphere opposite to that of observation for a short field line. Alternatively, it may correspond to any place along the field line. At this stage, we cannot identify the source univocally.

4.1. Temporal Variations or Spatial Structures?

As shown in Figure 2, the events can be clearly separated into two categories. The events selected in this study have positive slopes when observed in the Northern Hemisphere while they have negative slopes when they are observed in the Southern Hemisphere. Below, we present three scenarios to try to explain this pattern. The first two scenarios deal with the case of a spatial structure while the third scenario considers the case of temporal variations. We discuss each cases and illustrate them with a sketch, and we introduce the expected signatures a spacecraft would observe (Figure 9). Regardless of the case, we assume that there are particles with pitch angle continuously ranging between 0° and 180°. For simplicity, we do not consider the spatial extent of the source and how it maps at the spacecraft location. From the expected spacecraft observations, we present by elimination why the observations are more likely due to temporal variations rather than due to a spatial structure moving relative to the spacecraft. We finish this section by discussing consecutive PASSes.

We begin by dealing with the cases of spatial structuring which could be due to the $\mathbf{E} \times \mathbf{B}$ drift. Consider the Northern Hemisphere and particles being injected somewhere in the tail with the same energies but with pitch angles ranging from 0° to 90° (earthward moving particles). The more field-aligned particles take less time to cover a certain distance than the more perpendicular particles. Hence, the more perpendicular particles have more time to be affected by the southward $\mathbf{E} \times \mathbf{B}$ drift resulting in their gyrocenter being located closer to the neutral sheet than the gyrocenter of the particles with ∼0° pitch angle. Also, the gyrocenter of the reflected particles, now moving tailward, should be observed closer to the neutral sheet than when they were moving earthward. Concerning the Southern Hemisphere, the opposite structuring occurs because $B_X < 0$ and the $\mathbf{E} \times \mathbf{B}$ drift is northward. Therefore, the gyrocenter of the particles with 180° pitch angle would be closer to the lobes, and the gyrocenter of the more perpendicular particles would be closer to the neutral sheet.

Two cases arise from this spatial separation mechanism depending on the $\mathbf{E} \times \mathbf{B}$ drift velocity compared to the gyroradii of the particles. Indeed, if the $\mathbf{E} \times \mathbf{B}$ drift is small, the gyrocenters of particles with different pitch angles would not separate much spatially, and a large range of pitch angles could be observed simultaneously within the structure. On the other hand, if the $\mathbf{E} \times \mathbf{B}$ drift is large, the particles with different pitch angles would be separated in space, and a small range of pitch angles would be observed. The measured pitch angles would depend on the relative position of the structure and the satellite.

We present Figures 9a and 9b to illustrate the cases of a small and large $\mathbf{E} \times \mathbf{B}$ drift velocity, respectively. We constrain our example to the Northern Hemisphere with Earth located to the left. We schematically show the trajectories of ions with approximately 0° (orange), 45° (blue), 90° (red, represented as if they were moving earthward), 135° (blue), and 180° (orange) pitch angle, and the associated gyrocenters along the magnetic field lines are shown in light gray. We indicate the pitch angles (PA) of the particles to the right of the particles' gyrocenters. The vertical spacings between the magnetic field lines are due to the $\mathbf{E} \times \mathbf{B}$ drift. To the right of the pitch angles list, we show two possible relative spacecraft crossings and key times at which

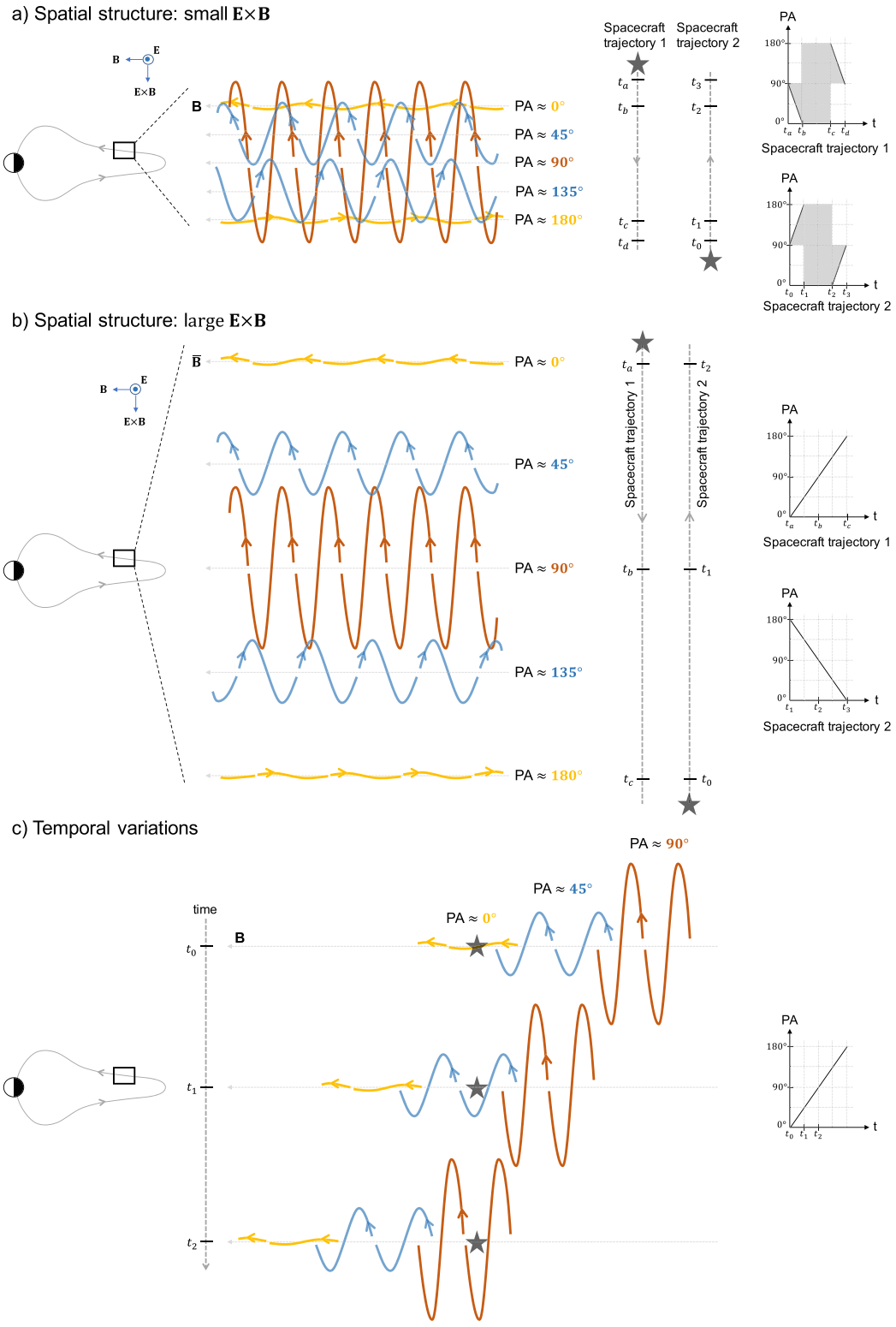

Figure 9. Illustration of the cases of spatial structures (a, b) and temporal variations (c) when observed in the Northern Hemisphere. The satellite is marked using a *star*. We present the trajectory of ions with approximately 0° (orange), 45° (blue), 90° (red, represented as if they were moving earthward), 135° (blue), and 180° (orange) pitch angle. In each case, the expected spacecraft signatures are shown on the right-hand side. (a) Small $\mathbf{E} \times \mathbf{B}$ drift and (b) large $\mathbf{E} \times \mathbf{B}$ drift as well as expected spacecraft crossing signatures. (c) Case of temporal variations and the expected spacecraft measurement of the structure.

the crossings occur; first from the lobe to the neutral sheet and then from the neutral sheet toward the lobe. Finally, to the uttermost right are schematics of the expected spacecraft signatures for the two crossings. The black lines indicate the general increase/decrease of the observed pitch angle during the crossings, and the gray areas represent the measurement of particles with a mixture of pitch angles.

As a first case of spatial structure, consider a small $\mathbf{E} \times \mathbf{B}$ drift velocity such that, even though the gyrocenters of particles with different pitch angles have been clearly separated, the particles have not (Northern Hemisphere case shown in Figure 9a). This is because the distance separating the gyrocenters due to the $\mathbf{E} \times \mathbf{B}$ drift velocity is smaller than the gyroradius of the particles involved. A spacecraft entering the structure from the top (i.e., lobe side) in Figure 9a would start by "remotely" probing the structure by observing the most perpendicular particles (t_a). This is because the gyroradius of a 90° pitch angle particle is larger than the spatial separation due to the $\mathbf{E} \times \mathbf{B}$ drift. As the spacecraft moves southward, it would start detecting particles that are more and more field aligned (t_b and black line to the uttermost right). Once the spacecraft enters the core of the structure, a mixture of all the pitch angles could be observed (gray area). As the spacecraft exits the structure (t_c), it observes pitch angles from 180° continuously decreasing down to finally only measure the particles with 90° pitch angle (t_d). Note that the order in which the particles are observed as the spacecraft exits the structure might change depending on the magnetic field between the satellite and Earth. These structures cannot explain PASS and even if the associated signatures occur, they have not been selected as follows from the selection criteria (section 2.3).

For the second case of spatial structure, consider a larger $\mathbf{E} \times \mathbf{B}$ drift velocity (Figure 9b). That is, a $\mathbf{E} \times \mathbf{B}$ drift velocity that is large enough to spatially separate the particles with increasing pitch angle. Note that we only represent a handful of particles while we assumed that there is a continuum of pitch angles. Therefore, the gaps without particles in our illustration (Figure 9b) are not representative of reality, and particles with intermediate pitch angles should be present. Unlike the first case, such spatial structure results in a monotonic spatial separation of the particles with different pitch angles with the most field-aligned particles closest to the lobes. Depending on the relative motion of the spacecraft and the structure, we could therefore observe either a change in pitch angle from 0° to 180° or from 180° to 0° regardless of the hemisphere. Hence, to observe the PASS slopes as in Figure 2, there needs to be a mechanism that would consistently be moving the structure over the spacecraft and toward the lobes (e.g., the thickening of the plasma sheet; Sergeev et al., 1998). Such motion would mean that, for every single PASS, the satellite should observe a decrease of B_X in the Northern Hemisphere and an increase of B_X in the Southern Hemisphere. Even though this is observed in the statistical result obtained from the superposed epoch analysis (Figure 7), a number of events have signatures opposite to those shown by the median in their hemisphere. This means that for those events, and if PASSes are spatial structures, they should have a "wrong" slope (i.e., disagreeing with the dominant pattern in Figure 2), but all the PASSes used in the superposed epoch analysis plot satisfy the clear pattern: positive PASS slopes in the Northern Hemisphere and negative PASS slopes in the Southern Hemisphere. Therefore, we do not think that PASSes are due to spatial structures.

Finally, we illustrate the case of temporal variations in Figure 9c. The time increases downward, and at each time stamp, we show the spacecraft position (*star*) and its surrounding. Illustrative trajectories of earthward particles with approximately 0° (orange), 45° (blue), and 90° (red) pitch angle are presented at each time stamps. To the right of the particles' trajectories, we present the expected spacecraft measurements.

In the case of temporal variations, the signatures would be due to the temporal delay of the arrival of particles with different properties (energies and pitch angles) at the spacecraft location (Figure 9c). Note that this is the interpretation provided in De Spiegeleer et al. (2019). We assume that the particles are emitted initially at the source during a fixed time interval. The fastest particles take a time t_0 to reach the spacecraft and the slower ones arrive later. That means that for a fixed energy, the first particles to arrive are the most field-aligned ones (closest to 0° pitch angle) while the particles that are slower and more perpendicular are yet to reach the spacecraft. At time t_1, the fastest particles are between their mirror point and the spacecraft, and the slightly more perpendicular particles (blue) are now being detected by the spacecraft. This continues as time increases. Once the particles have reached their mirror point, they move back toward the tail and over the spacecraft. The exact time when the tailward moving particles are observed by the spacecraft depends on the magnetic geometry between the satellite and the mirror point of the particles.

We think that the interpretation of PASSes being due to temporal variations is the most reasonable as it is consistent with the majority of the PASSes signatures without major assumptions. In addition, De Spiegeleer

et al. (2019) used a model magnetosphere to trace forward in time the observed earthward moving particles. It was found that the particles traveled back near the spacecraft location in a time agreeing with the spacecraft observations. On the other hand, if the structure was spatial, the precise times at which the particle flux enhancements would be observed in the pitch angle-time spectrogram would depend on the relative speed of the satellite and the structure. The matching results of the simulation would then be pure coincidence.

Sometimes, consecutive PASSes are observed (Figure 3). This can be caused either by temporal variations or by spatially separated PASSes. A possible scenario in the case of temporal variations is that the spacecraft observes consecutive PASSes because the source accelerates the particles sporadically. In the case of spatial structures, two schemes are possible. First, there may be several sources on different field lines. The spatial separation between the sources would result in the spatial separation of where PASSes can be observed. Second, there may be a single moving source in the tail energizing the particles sporadically. The particles would then be accelerated at different places in the tail due to the motion of the source. PASSes would be observed at different Z depending on the location of the source when the particles were accelerated.

4.2. Velocity

The velocity used for the superposed epoch analysis in section 4.2 is the bulk velocity calculated from the distribution function measured by C4. This means that the velocity in the perpendicular direction does not only include the $\mathbf{E} \times \mathbf{B}$ drift but also all the general force drifts as well as the diamagnetic "drift". The $\mathbf{E} \times \mathbf{B}$ drift usually dominates in the magnetotail, but the diamagnetic drift can also have a non-negligible contribution (e.g., Hori et al., 2000). We investigate whether the signatures observed in $\delta V_{\perp Z}$ in section 4.2 can be due to the diamagnetic drift. The diamagnetic drift for a species with electric charge q in a magnetic field $\mathbf{B}$ due to a pressure gradient ∇p and with a density n can be expressed as $\mathbf{v}_d = -\frac{\nabla p \times \mathbf{B}}{qn\mathbf{B}^2}$. In the magnetotail, B_X is expected to be the dominant component. Hence, $\partial_y p < 0$ is required to observe a positive $\delta V_{\perp Z}$ in the Northern Hemisphere. Similarly in the Southern Hemisphere where $B_X < 0$, $\partial_y p < 0$ is also required to observe a negative $\delta V_{\perp Z}$. In our case, we study localized structures in the tail which have higher density than the surrounding plasma (not shown). Given an equation of state of the form $p = Cn^\gamma$, relating the pressure to the density with C and γ two constants, ∇p is always directed in the direction in which the density increases, that is toward the structure. Hence, probing where $\partial_y p < 0$ would mean that the spacecraft is consistently measuring on the dusk side of the structure, that is, at larger Y than where the structure is. This is unlikely to happen, and we therefore do not think that the diamagnetic drift plays a significant role in the velocity signatures presented in Figure 6.

4.3. Magnetic Field

The magnetic field signatures observed at the same time as PASSes may shed light on the acceleration mechanism(s). Understanding the relation between the particle and magnetic field data is therefore important. A decrease in the magnetic field magnitude is observed during PASSes. It corresponds mostly to a decrease (increase) of B_X in the Northern (Southern) Hemisphere but also possibly to a decrease of B_Z (Figure 7). Again, we emphasize that the magnetic field signatures in Figure 7 are deviations to the background magnetic field. Here, we discuss two possible schemes for the particle and the magnetic field data to be related. The first explanation relies on the pressure balance between the particle pressure and the magnetic pressure while the second explanation rest upon the relative motion of the plasma sheet and the satellite.

To have pressure balance would mean that the sum of the plasma pressure and the magnetic pressure is constant. A decrease in the magnetic pressure during PASSes is observed in the superposed epoch analysis (Figure 10a). The clear dip in the superposed epoch analysis of the magnetic pressure P_B reaches a minimum value of −16 pPa. Also, it is without surprise to observe an increase in the O^+ pressure P_{O^+} (Figure 10b) and the H^+ pressure P_{H^+} (Figure 10c) as there is an increase of the particles' densities associated with the increased particle fluxes. However, note that the largest increase is observed for H^+ and not O^+. These three pressures can be combined for each PASS event to investigate the typical behavior of the total pressure using the superposed epoch analysis (Figure 10d). But a small dip reaching −4 pPa remains during the time of PASS. It is unclear whether it is significant or not. In any case, the plasma pressure can account for most, if not all, of the decrease in the magnetic pressure and one could argue that the decrease in the magnetic field is to maintain the pressure balance. However, pressure balance may not be exact during PASSes since it is derived from the single fluid equations and requires a number of assumptions. Among these are the assumptions that the magnetic geometry is planar and that the plasma is stationary. The planarity of the magnetic geometry may hold in the stretched magnetotail as long as the observations are made afar from

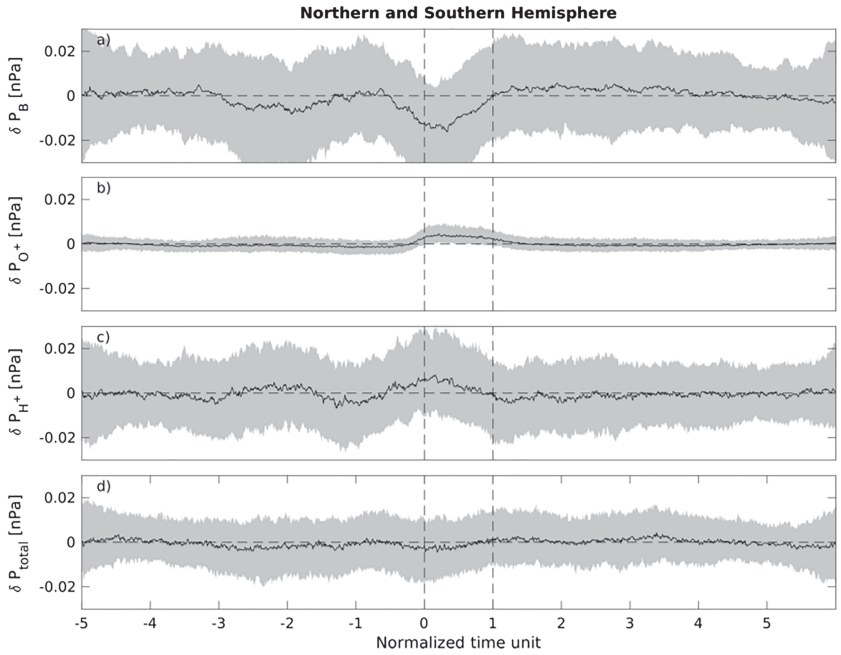

Figure 10. Superposed epoch analysis of the perturbation of (a) the magnetic pressure, (b) the O^+ pressure, (c) the H^+ pressure, and (d) the total pressure. The total pressure is the sum of the magnetic pressure, the O^+ pressure, and the H^+ pressure.

the neutral sheet. But, if PASSes are due to the sudden arrival of particles, the stationarity assumption would not be met, and the pressure balance would not hold exactly.

An alternative scenario that could explain the magnetic field signatures is the following. The signatures may be due to the relative motion of the spacecraft and the neutral sheet. If the spacecraft travels closer to the neutral sheet, B decreases and B_X decreases (increases) in the Northern (Southern) Hemisphere. Regarding B_Z, it should increase when the spacecraft moves closer to the neutral sheet, and it should decrease when the spacecraft moves away from it. This is not clearly observed in Figure 7d, but the variation of B_Z compared to its background value is slightly positive from −1 to 0 normalized time unit while it is negative afterward. This might correspond to the expected increase and decrease of B_Z associated with C4 moving closer and then away from the neutral sheet. This interpretation of the magnetic field signatures due to the relative motion of the spacecraft toward the neutral sheet and away from it may result from the thickening followed by the thinning of the plasma sheet (e.g., Panov et al., 2010; Sergeev et al., 1998). This is supported by the changes observed in the H^+ and O^+ perpendicular velocity along Z from Figures 6e and 6f. There is an increase of $V_{\perp Z}$ in the Northern Hemisphere (Figures 6e and 6g) and a decrease of $V_{\perp Z}$ in the Southern Hemisphere (Figures 6f and 6h). In the Northern Hemisphere, when $V_{\perp Z}$ increases, B and B_X decrease (Figures 7a and 7b). Then, $V_{\perp Z}$, B, and B_X recover simultaneously to their background values. On the other hand, the slight time shift in the $V_{\perp Z}$ signatures between the Northern and Southern Hemispheres (Figures 6e–6h) result in a time shift between the magnetic field signatures (Figures 7a and 7c), and the variations in $V_{\perp Z}$ (Figures 6f and 6h) compared to the observations in the Northern Hemisphere. The small difference in timing between the hemispheres could be due to the statistical variance of the selected events. A possible way for this scenario to hold is that the source that injects the particles forming PASSes might also affect the global geometry of the plasma sheet by thickening it.

The acceleration mechanism resulting in the enhanced particle flux still remains elusive. More detailed studies are required to investigate what the source(s) is (are). For example, to verify whether or not the observed O^+ originates directly from the ionosphere, simultaneous observation of a PASS and the ionosphere at the PASS footpoints is necessary. Or if in fact the particles are accelerated at reconnection, simultaneous observation of reconnection and PASS would be required. Such observations could also be supported using in-depth simulations. Clearly, a fortuitous case study accompanied by an in-depth simulation would be

required to univocally identify the source responsible for the acceleration of particles forming the PASSes which, in turn, produce flow reversal.

Acknowledgments
We thank the FGM and CIS teams as well as the Cluster Science Archive (CSA) for providing calibrated Cluster data. We also thank the World Data Center for Geomagnetism, Kyoto, for the AE index data. All data can be accessed online (https://www.cosmos.esa.int/web/csa, https://omniweb.gsfc.nasa.gov/, and http://wdc.kugi.kyoto-u.ac.jp/). A. D. S. and M. H. acknowledge support by the grants from the Swedish National Space Agency, Projects 105/14 and 271/14.. T. P. acknowledges support by the grants from the Swedish National Space Agency, Project 118/17, and the National Natural Science Foundation China, Project 41750110486. H. G. acknowledges the support by the Belgian Science Policy Office through the Solar Terrestrial Centre of Excellence, PRODEX/Cluster Contract 13127/98/NL/VJ(IC)-PEA90316 and BRAIN-Be Contract BR/175/A2/MOMA. We thank both reviewers for providing insightful comments that improved the quality of this article.

References

Alfvén, H. (1943). On the existence of electromagnetic-hydrodynamic waves. *Arkiv för Matematik, Astronomi Och Fysik*, *29*, 1–7.

Balogh, A., Carr, C. M., Acuña, M. H., Dunlop, M. W., Beek, T. J., Brown, P., et al. (2001). The Cluster Magnetic Field investigation: Overview of in-flight performance and initial results. *Annales Geophysicae*, *19*(10/12), 1207–1217. https://doi.org/10.5194/angeo-19-1207-2001

Baumjohann, W., Paschmann, G., & Cattell, C. A. (1989). Average plasma properties in the central plasma sheet. *Journal of Geophysical Research*, *94*(A6), 6597–6606. https://doi.org/10.1029/JA094iA06p06597

Birn, J., Nakamura, R., Panov, E. V., & Hesse, M. (2011). Bursty bulk flows and dipolarization in mhd simulations of magnetotail reconnection. *Journal of Geophysical Research*, *116*, A01210. https://doi.org/10.1029/2010JA016083

Davis, T. N., & Sugiura, M. (1966). Auroral electrojet activity index ae and its universal time variations. *Journal of Geophysical Research*, *71*(3), 785–801. https://doi.org/10.1029/JZ071i003p00785

De Spiegeleer, A., Hamrin, M., Gunell, H., Volwerk, M., Andersson, L., Karlsson, T., et al. (2019). Oscillatory flows in the magnetotail plasma sheet: Cluster observations of the distribution function. *Journal of Geophysical Research: Space Physics*, *124*, 2736–2754. https://doi.org/10.1029/2018JA026116

Dungey, J. W. (1961). Interplanetary magnetic field and the auroral zones. *Physical Review Letters*, *6*, 47–48. https://doi.org/10.1103/PhysRevLett.6.47

Eastman, T. E., Frank, L. A., Peterson, W. K., & Lennartsson, W. (1984). The plasma sheet boundary layer. *Journal of Geophysical Research*, *89*(A3), 1553–1572. https://doi.org/10.1029/JA089iA03p01553

Eastwood, J. P., Phan, T. D., Øieroset, M., & Shay, M. A. (2010). Average properties of the magnetic reconnection ion diffusion region in the earth's magnetotail: The 2001-2005 Cluster observations and comparison with simulations. *Journal of Geophysical Research*, *115*, A08215. https://doi.org/10.1029/2009JA014962

Escoubet, C. P., Fehringer, M., & Goldstein, M. (2001). Introduction the Cluster mission. *Annales Geophysicae*, *19*(10/12), 1197–1200. https://doi.org/10.5194/angeo-19-1197-2001

Hori, T., Maezawa, K., Saito, Y., & Mukai, T. (2000). Average profile of ion flow and convection electric field in the near-earth plasma sheet. *Geophysical Research Letters*, *27*(11), 1623–1626. https://doi.org/10.1029/1999GL003737

Juusola, L., Østgaard, N., & Tanskanen, E. (2011). Statistics of plasma sheet convection. *Journal of Geophysical Research*, *116*, A08201. https://doi.org/10.1029/2011JA016479

Panov, E. V., Baumjohann, W., Kubyshkina, M. V., Nakamura, R., Sergeev, V. A., Angelopoulos, V., et al. (2014). On the increasing oscillation period of flows at the tailward retreating flux pileup region during dipolarization. *Journal of Geophysical Research: Space Physics*, *119*, 6603–6611. https://doi.org/10.1002/2014JA020322

Panov, E. V., Nakamura, R., Baumjohann, W., Sergeev, V. A., Petrukovich, A. A., Angelopoulos, V., et al. (2010). Plasma sheet thickness during a bursty bulk flow reversal. *Journal of Geophysical Research*, *115*, A05213. https://doi.org/10.1029/2009JA014743

Pitkänen, T., Aikio, A. T., Amm, O., Kauristie, K., Nilsson, H., & Kaila, K. U. (2011). Eiscat-Cluster observations of quiet-time near-earth magnetotail fast flows and their signatures in the ionosphere. *Annales Geophysicae*, *29*(2), 299–319. https://doi.org/10.5194/angeo-29-299-2011

Rème, H., Aoustin, C., Bosqued, J. M., Dandouras, I., Lavraud, B., Sauvaud, J. A., et al. (2001). First multispacecraft ion measurements in and near the Earth's magnetosphere with the identical Cluster ion spectrometry (CIS) experiment. *Annales Geophysicae*, *19*(10/12), 1303–1354. https://doi.org/10.5194/angeo-19-1303-2001

Roberts, B. (1981). Wave propagation in a magnetically structured atmosphere. *Solar Physics*, *69*(1), 39–56. https://doi.org/10.1007/BF00151254

Sauvaud, J.-A., & Kovrazhkin, R. A. (2004). Two types of energy-dispersed ion structures at the plasma sheet boundary. *Journal of Geophysical Research*, *109*, A12213. https://doi.org/10.1029/2003JA010333

Sergeev, V., Angelopoulos, V., Carlson, C., & Sutcliffe, P. (1998). Current sheet measurements within a flapping plasma sheet. *Journal of Geophysical Research*, *103*(A5), 9177–9187. https://doi.org/10.1029/97JA02093

Sergeev, V., Runov, A., Baumjohann, W., Nakamura, R., Zhang, T. L., Balogh, A., et al. (2004). Orientation and propagation of current sheet oscillations. *Geophysical Research Letters*, *31*, L05807. https://doi.org/10.1029/2003GL019346

Turkakin, H., Mann, I., & Rankin, R. (2014). Kelvin-Helmholtz unstable magnetotail flow channels: Deceleration and radiation of mhd waves. *Geophysical Research Letters*, *41*, 3691–3697. https://doi.org/10.1002/2014GL060450